Resonant adiabatic passage with three qubits

Sangchul Oh, Yun-Pil Shim, Jianjia Fei, Mark Friesen, and Xuedong Hu

Resonant Adiabatic Passage with Three Qubits

Sangchul Oh,[1] Yun-Pil Shim,[2] Jianjia Fei,[2] Mark Friesen,[2] and Xuedong Hu[1]

[1]*Department of Physics, University at Buffalo, The State University of New York, Buffalo, New York 14260-1500, USA*
[2]*Department of Physics, University of Wisconsin-Madison, Madison, Wisconsin 53706, USA*
(Dated: January 11, 2013)

We investigate the non-adiabatic implementation of an adiabatic quantum teleportation protocol, finding that perfect fidelity can be achieved through resonance. We clarify the physical mechanisms of teleportation, for three qubits, by mapping their dynamics onto two parallel and mutually-coherent adiabatic passage channels. By transforming into the adiabatic frame, we explain the resonance by analogy with the magnetic resonance of a spin-1/2 particle. Our results establish a fast and robust method for transferring quantum states, and suggest an alternative route toward high precision quantum gates.

Fault-tolerant quantum computation requires high-precision quantum gates with noise thresholds between 10^{-4} and 10^{-2}, depending on the fault-tolerance scheme [1, 2]. This stringent requirement poses significant technical challenges, even for the more mature qubit architectures, such as those based on trapped ions [3]. Identifying gate protocols that are both fast and robust is therefore an important research objective for quantum information processing.

One potential approach to robust quantum gates is based on the adiabatic principle – a fundamental tenet of quantum mechanics [4]. According to the adiabatic theorem, a quantum system in an eigenstate remains there, provided that the Hamiltonian varies slowly in time. Applications of the adiabatic theorem include the Born-Oppenheimer approximation and the Landau-Zener-Stückelberg-Majorana transition at an avoided crossing [5–8], the latter having been demonstrated in both superconducting and spin qubits [9, 10]. Other experimental implementations include adiabatic population transfers between two or three-level systems, known as adiabatic passages (AP) [11–14], which have been demonstrated in atomic, molecular, and optical devices. There are also theoretical proposals for realizing AP with superconducting qubits [15] and quantum dot arrays [16]. Adiabatic quantum information processing [17] entails the adiabatic transformation of the ground state of an initial Hamiltonian into that of a target Hamiltonian. Compared to the quantum circuit model, adiabatic gates are resistant to decoherence when a finite excitation gap persists throughout the evolution, and they are robust to gating errors, by virtue of adiabaticity. This can be a drawback however, since the maximum speed of an adiabatic gate is also proportional to the spectral gap.

In this paper we investigate a non-adiabatic form of adiabatic quantum teleportation (AQT). Conventional AQT was proposed in the context of fault tolerant quantum computation [18]. Here, we focus on systems with three qubits, where we can solve the evolution analytically. We show that resonances occur, enabling high-fidelity teleportation that is both fast and quite robust against timing errors in the absence of decoherence. This interesting effect can be explained in the language of spin resonance, by transforming into the adiabatic frame. Our results point toward a possible new paradigm for quantum algorithms, based on fast adiabatic gates. Our work also provides an intriguing mapping between three coupled qubits and a three-level atom, which could lead to further spin analogies from atomic Λ-system physics. The experimental requirements for implementing AQT have already been demonstrated in the laboratory for triple quantum dots [10] and superconducting circuits [19]. Our results could therefore be tested immediately.
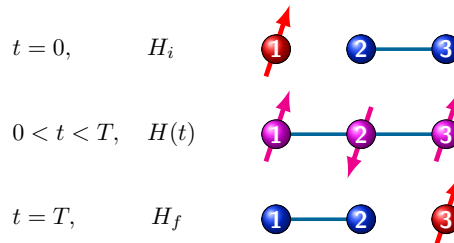

Figure 1: (color online). The couplings and the information distribution (by color and arrow) among three qubits are shown at the initial, intermediate, and final stages of adiabatic quantum teleportation.

The adiabatic quantum teleportation protocol is illustrated in Fig. 1. Initially, qubit 1 is isolated and prepared in an arbitrary superposed state, while qubits 2 and 3 are coupled, as described below, and prepared in the maximally entangled singlet state. The antiferromagnetic coupling between qubits 1 and 2 (2 and 3) is then turned on (off) slowly. When the evolution is complete, the quantum state of qubit 1 will be teleported to qubit 3. As proposed in Ref. [18], the scheme succeeds when the run time T satisfies the adiabatic theorem.

To explore non-adiabatic effects, we solve the exact dynamics of the three-qubit system. It is governed by a time-dependent Hamiltonian, which smoothly changes from the initial Hamiltonian H_i at $t = 0$ to the final

Hamiltonian H_f at $t = T$:

$$H(t) = f(t)\,H_i + g(t)\,H_f\,. \tag{1}$$

The initial and final Hamiltonians are given by

$$H_i = J\left(\sigma_{2x}\,\sigma_{3x} + \sigma_{2y}\,\sigma_{3y} + \gamma\,\sigma_{2z}\,\sigma_{3z}\right), \tag{2a}$$

$$H_f = J\left(\sigma_{1x}\,\sigma_{2x} + \sigma_{1y}\,\sigma_{2y} + \gamma\,\sigma_{1z}\,\sigma_{2z}\right), \tag{2b}$$

where $\sigma_{i\mu}$ are the Pauli operators with $i = 1, 2, 3$ and $\mu = x, y, z$, and J is the strength of the qubit-qubit coupling. The anisotropy parameter $\gamma = 0$ corresponds to an *XX* coupling, available in superconducting qubits, while $\gamma = 1$ corresponds to the isotropic Heisenberg coupling of spin qubits. The interpolation or switching functions $f(t)$ and $g(t)$ satisfy $f(0) = g(T) = 1$ and $f(T) = g(0) = 0$. Here we consider two ways to connect H_i to H_f: (i) a linear interpolation with $f(t) = 1 - t/T$ and $g(t) = t/T$, and (ii) a harmonic interpolation with $f(t) = \cos(\pi t/2T)$ and $g(t) = \sin(\pi t/2T)$.

AQT begins with an initial three-qubit state given by

$$|\psi(0)\rangle = \left(a|0\rangle + b|1\rangle\right)_1 \otimes \frac{1}{\sqrt{2}}\left(|01\rangle - |10\rangle\right)_{2,3}, \tag{3}$$

where $a|0\rangle + b|1\rangle$ is the arbitrary state to be teleported. The success of AQT is measured by the fidelity $F(T) = |\langle\psi_T|\psi(T)\rangle|^2$ where $|\psi(T)\rangle$ is the final state at time T and $|\psi_T\rangle = \frac{1}{\sqrt{2}}\left(|01\rangle - |10\rangle\right)_{1,2} \otimes \left(a|0\rangle + b|1\rangle\right)_3$ is the target state. The dynamics of AQT is governed by the time-dependent Hamiltonian (1), with the initial state (3).

Hamiltonian (1) satisfies the commutation relation $[H(t), S_z] = 0$, so that the z-component of the total spin angular momentum $S_z \equiv \frac{1}{2}\left(\sigma_{1z} + \sigma_{2z} + \sigma_{3z}\right)$ is a good quantum number, which is conserved during evolution. The three-qubit Hamiltonian (1) is thus block-diagonal:

$$H(t) = \underbrace{H_3}_{\text{up}} \oplus \underbrace{H_3}_{\text{down}} \oplus H_1 \oplus H_1\,. \tag{4}$$

The two H_1 operators act on $|000\rangle$ and $|111\rangle$, while the two H_3 operators act on the distinct subspaces $\mathcal{H}_{1/2} = \mathrm{Span}(|100\rangle, |010\rangle, |001\rangle)$ and $\mathcal{H}_{-1/2} = \mathrm{Span}(|011\rangle, |101\rangle, |110\rangle)$, and have the same form

$$H_3(t) = J\begin{bmatrix} (f-g)\gamma & 2g & 0 \\ 2g & -(f+g)\gamma & 2f \\ 0 & 2f & -(f-g)\gamma \end{bmatrix}. \tag{5}$$

Interestingly, H_3 is also the AP Hamiltonian for a 3-level atom [12–14], with the switching functions $f(t)$ and $g(t)$ being the Stokes and pump pulses in the context of AP. For the initial states we consider, the H_1 operators are never involved in the system evolution. The AQT protocol therefore consists of two parallel, identical and mutually-coherent APs governed by H_3, corresponding to the $S_z = \pm\frac{1}{2}$ components of the three-qubit system.

To understand the dynamics of AQT, we solve the time-dependent Schrödinger equation with Hamiltonian

(5) in two ways. First, we consider the adiabatic limit, for which there is a mapping between AQT and two mutually-coherent APs. Second, we obtain numerical solutions (and in one case, an analytical solution) for finite T. We also consider the separate cases of *XX* and Heisenberg couplings.

The adiabatic theorem states that, starting from an eigenstate $|E_n(0)\rangle$, the adiabatically evolved state $|\psi(t)\rangle \simeq e^{-i/\hbar \int_0^t E_n(t')\,dt' + \gamma_B}|E_n(t)\rangle$ is simply an instantaneous eigenstate, up to a phase factor. Here, γ_B is the Berry phase, and E_n and $|E_n\rangle$ are the instantaneous eigenvalues and eigenstates of $H_3(t)$, defined by

$$H_3(t)\,|E_n(t)\rangle = E_n(t)\,|E_n(t)\rangle\,. \tag{6}$$

Solving Eq. (6) for an *XX* coupling ($\gamma = 0$), gives the instantaneous energy levels $E_0(t) = 0$ and $E_\pm(t) = \pm 2J\sqrt{f^2 + g^2}$, with the corresponding eigenstates

$$|E_0(t)\rangle = \begin{bmatrix} \cos\theta \\ 0 \\ -\sin\theta \end{bmatrix}, \quad |E_\pm(t)\rangle = \frac{1}{\sqrt{2}}\begin{bmatrix} \sin\theta \\ \pm 1 \\ \cos\theta \end{bmatrix}. \tag{7}$$

Here, the mixing angle $\theta = \tan^{-1}[g(t)/f(t)]$ runs from 0 to $\pi/2$ as time t goes from 0 to T. For the Heisenberg coupling ($\gamma = 1$), the instantaneous energy levels are $E_0(t)/J = (f + g)$ and $E_\pm(t)/J = [-f - g \pm 2\sqrt{f^2 - fg + g^2}]$, with the corresponding eigenstates

$$|E_0(t)\rangle = \frac{1}{\sqrt{3}}\begin{bmatrix} 1 & 1 & 1 \end{bmatrix}^T, \tag{8a}$$

$$|E_\pm(t)\rangle = \frac{1}{\sqrt{\mathcal{N}}}\begin{bmatrix} \sin\theta \\ -\cos\theta \pm \sqrt{1 - \cos\theta\sin\theta} \\ \cos\theta - \sin\theta \mp \sqrt{1 - \cos\theta\sin\theta} \end{bmatrix}, \tag{8b}$$

where $\mathcal{N} \equiv 2(2\cos\theta - \sin\theta)\sqrt{q} + 4q$, $q = 1 - \cos\theta\sin\theta$.

Equation (5) governs the evolution of both AQT and conventional AP, as depicted in Fig. 2. For AP, the population of a Λ-type system is transferred from state $|1\rangle$ to $|3\rangle$, while state $|2\rangle$ remains unpopulated [12–14]. Paradoxically, the AP pulse sequence appears to occur in reverse order (S followed by P), as shown in panel (a). The instantaneous eigenstate used in this evolution is $|E_0(t)\rangle$ from Eq. (7). For AQT, on the other hand, the instantaneous eigenstate used is $|E_-\rangle$ in Eqs. (7) or (8), leading to slight differences between panels (a) and (b). In panels (b) and (c), we see that the "up" state ($|0\rangle$) is transferred from the left-most qubit to the right-most qubit, following a similarly counter-intuitive pulse sequence. Since the H_3 operators are identical for the subspaces $\mathcal{H}_{1/2}$ and $\mathcal{H}_{-1/2}$, their separate evolutions are also identical. Thus, as illustrated in Fig. 1, an arbitrary state $a|0\rangle + b|1\rangle$ of qubit 1 in Eq. (3) is transmitted to qubit 3 via two mutually-coherent evolutions.

The adiabatic solution described above is only valid when $JT/\hbar \gg 1$. In this limit, Eqs. (7) and (8) give a perfect (adiabatic) fidelity, $F_{\mathrm{ad}}(T) = 1$. When T is finite however, the adiabatic theorem predicts that
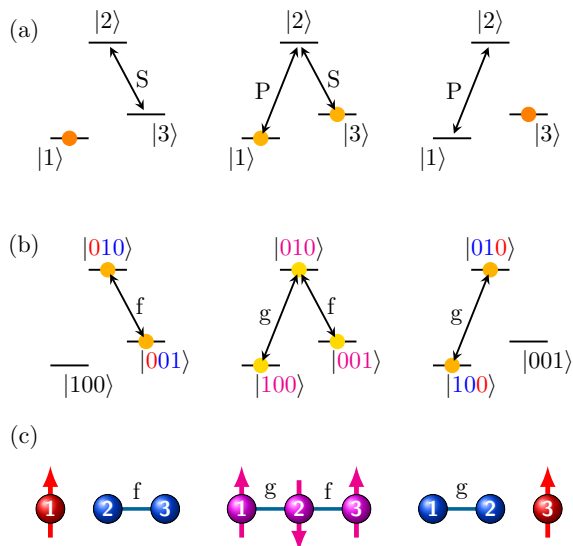
Figure 2: (color online). Adiabatic passage protocols for (a) Λ-type levels, (b) the "up" component (red $|0\rangle$) of a 3-qubit system, and (c) the corresponding spin configurations. From right to left: the initial, intermediate, and final stages of evolution. In (a) and (b), filled circles represent populations of levels. S and P stand for the Stokes and pump pulses.

Figure 3: (color online). Infidelity $1 - F$ is plotted as a function of $JT/\pi\hbar$ for (a) XX and (b) Heisenberg couplings, using harmonic and linear interpolation functions (solid red and dotted blue lines, respectively). The black dashed line represents $1 - F \propto 1/(JT/\hbar)^2$ for comparison. (c) The infidelity of a conventional swap operation or Rabi oscillation (if $2J$ is replaced by $\mu_B B_x$) is given by $1 - F = \cos^2(2JT/\hbar)$. Windows of tolerable timing errors to get $1 - F \leq 10^{-2}$ are indicated by blue shaded regions for (c) conventional swap gates vs. (d) AQT with XX coupling and harmonic interpolation shown in (a). For (d), the robustness improves monotonically in the adiabatic limit, and always surpasses the robustness in (c).

$1 - F \propto (JT/\hbar)^{-2}$, with possibly oscillatory modifications [6, 20, 21]. To obtain an infidelity $1 - F < 10^{-6}$, the adiabatic gate time should be $JT/\hbar \sim \mathcal{O}(10^3)$, *much* longer than a conventional gate, for which $JT/\hbar \sim \mathcal{O}(1)$. Such slow adiabatic evolution could obviously cause problems, despite its intrinsic fault tolerance. However, when we perform a numerical integration of the time-dependent Schrödinger equation governed by Hamiltonian (5), we find that the infidelity $1 - F$ as a function of evolution time T is far from a smooth quadratic function. Instead, while it approaches the predicted upper envelope, there are also striking resonance features where the infidelity dips to zero, as shown in Fig. 3 (a) and (b). Furthermore, as illustrated in Fig. 3(d), the timing requirement for this adiabatic protocol, even when it is run non-adiabatically, is much more relaxed compared to that for a conventional Rabi type of gate shown in Fig. 3(c). Indeed, Fig. 3(d) shows that when $JT/\hbar > 4\pi$, which could still be a reasonably short evolution time, there is no timing requirement at all for our protocol if the required fidelity is 99%. This is in clear contrast with (and clearly superior over) the conventional Rabi-type gates, which has a fixed timing requirement [Fig. 3(c)] given a Rabi pulse intensity.

The origin of the unexpected resonances in AQT fidelity becomes clear when we consider the XX coupling with harmonic interpolation functions. For this special case, we can obtain an analytical solution by transforming into the adiabatic frame [22], as illustrated in Fig. 4. We define

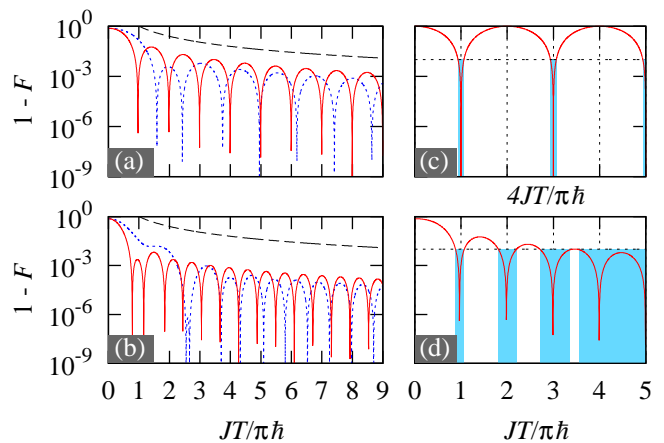$$D(t) = A^{-1}(t)H_3(t)A(t), \quad |\psi(t)\rangle = A(t)|\phi(t)\rangle, \quad (9)$$

where the column vectors of $A(t)$ are the instantaneous eigenstates given by Eq. (7). The Schrödinger equation in the adiabatic frame takes the form

$$i\hbar\frac{\partial}{\partial t}|\phi(t)\rangle = \left[D(t) - i\hbar A^{-1}(t)\frac{\partial A(t)}{\partial t}\right]|\phi(t)\rangle, \quad (10a)$$

$$= H_{\text{tr}}|\phi(t)\rangle. \quad (10b)$$

For harmonic interpolation and XX couplings, the transformed Hamiltonian H_{tr} becomes time-independent:

$$H_{\text{tr}} = 2J\begin{bmatrix} -1 & 0 & 0 \\ 0 & 0 & 0 \\ 0 & 0 & 1 \end{bmatrix} + \frac{\pi\hbar}{2T}\frac{1}{\sqrt{2}}\begin{bmatrix} 0 & i & 0 \\ -i & 0 & -i \\ 0 & i & 0 \end{bmatrix} \quad (11a)$$

$$= \hbar\omega_0\,Z + \hbar\omega_1\,Y', \quad (11b)$$

where $\hbar\omega_0 \equiv 2J$ is the absolute value of the ground state energy and $\omega_1 \equiv \pi/2T$ is the frequency of the switching functions, $f(t) = \cos(\omega_1 t)$ and $g(t) = \sin(\omega_1 t)$. The matrix Y', which resembles the angular momentum operator I_y of a spin-1 system, is responsible for the non-adiabatic behavior. It has the same eigenvalues as Z, i.e., 0 and ± 1. The Hamiltonian in the adiabatic frame, $H_{\text{tr}} = \hbar\Omega(Z\cos\alpha + Y'\sin\alpha)$, has the eigenvalues

$$e_0 = 0, \; e_\pm = \pm\hbar\Omega, \quad \text{with} \quad \Omega \equiv \sqrt{\omega_0^2 + \omega_1^2}, \quad (12a)$$

and the corresponding eigenstates

$$|e_0\rangle = \frac{1}{\sqrt{2}}\begin{bmatrix} -\sin\alpha \\ i\sqrt{2}\cos\alpha \\ \sin\alpha \end{bmatrix}, |e_\pm\rangle = \frac{1}{2}\begin{bmatrix} 1 \mp \cos\alpha \\ \mp i\sqrt{2}\sin\alpha \\ 1 \pm \cos\alpha \end{bmatrix}, \quad (12b)$$

where $\tan\alpha \equiv \omega_1/\omega_0$.

As illustrated in Fig. 4, the time evolution in the adiabatic frame is analogous to the rotation of a spin-1 system around an effective, constant magnetic field given by $\mathbf{\Omega} = \omega_0 \hat{\mathbf{Z}} + \omega_1 \hat{\mathbf{Y}}'$, where $\hat{\mathbf{Y}}'$ is the rotation axis associated with matrix Y'. The state vector is initially oriented along $\hat{\mathbf{Z}}$, which corresponds to $|E_-(t)\rangle$ in the original frame of Eqs. (7). In the adiabatic limit $\omega_0 \gg \omega_1$, the precession axis is $\hat{\mathbf{\Omega}} = \hat{\mathbf{Z}}$, so the state vector does not precess. Thus, in the original frame, the state vector is given by $|E_-(t)\rangle$ for all t.

Non-adiabatic evolution occurs when $\omega_1 > 0$. The state vector is initially aligned with $\hat{\mathbf{Z}}$ in the adiabatic frame; however it precesses when $\hat{\mathbf{\Omega}} \neq \hat{\mathbf{Z}}$. As the state vector deviates from $\hat{\mathbf{Z}}$ in the adiabatic frame, it also deviates from the adiabatic ground state $|E_-(t)\rangle$ in the original frame. After a full precession period given by $\Omega T = 2\pi n$, the state vector returns to the $\hat{\mathbf{Z}}$ direction, or the ideal target state $|E_-(T)\rangle$. The physical picture is analogous to the magnetic resonance of a spin-1/2 particle in a static magnetic field, with a small perpendicular ac field. In this case, the state vector precesses about a static magnetic field in the rotating frame [23, 24].
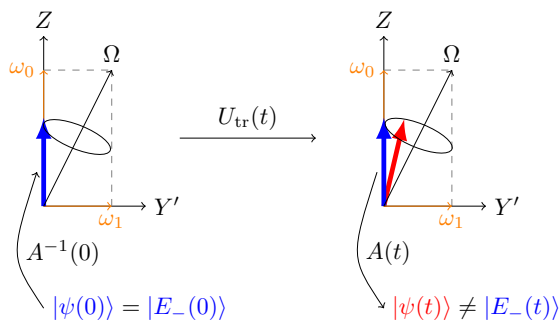

Figure 4: (color online). Schematic representation of the time evolution in the adiabatic frame, given by Eq. (13). The instantaneous eigenvector is represented by a thick blue arrow and the exact evolved state by a thick red arrow.

As depicted in Fig. 4, the evolved state in the original frame is given by

$$|\psi(t)\rangle = A(t)\, U_{\text{tr}}(t)\, A^{-1}(0)\, |\psi(0)\rangle, \qquad (13)$$

where the time evolution operator in the adiabatic frame is given by $U_{\text{tr}} = e^{-iH_{\text{tr}}t/\hbar}$. The fidelity at time $t = T$ can be obtained exactly:

$$F(T) = \frac{1}{4}\Big[\cos^2(\Omega T)(1 + \cos^2\alpha)^2 + 4\sin^2(\Omega T)\cos^2\alpha$$
$$+ 2\cos(\Omega T)\sin^2\alpha(1 + \cos^2\alpha) + \sin^4\alpha \Big]. \qquad (14)$$

The results are indistinguishable from the numerical solution shown in Fig. 3(a). Perfect fidelity occurs at the resonance condition $\Omega T = 2\pi n$, which is given by

$$JT/\hbar\pi = \sqrt{n^2 - \frac{1}{16}} \approx n, \quad n \in \mathbb{N}. \qquad (15)$$

We have now identified two paths to perfect teleportation. The first corresponds to the asymptotic (adiabatic) limit on the far right-hand side of Fig. 3 (a) or (b). The second occurs at any one of the resonant conditions. Furthermore, Fig. 3 (c) and (d) clearly show that compared to the conventional swap gates, the resonant adiabatic teleportation protocol is very robust, especially for somewhat longer (but still far from adiabatic) gate times. It is interesting that resonances only occur in certain interpolation schemes. For example, the quadratic interpolation $f(s) = 1 - s^2$ and $g(s) = s(2 - s)$ has resonances, while $f(s) = 1 - s^2$ and $g(s) = s^2$ does not.

We now examine how the AQT protocol is affected by external magnetic fields. For simplicity, we assume the external magnetic fields applied to three spins are aligned in the same direction, i.e., in z-direction. The $S_z = \pm 1/2$ channels are then still completely decoupled from each other in the AQT protocol. We first consider a uniform magnetic field B_0. The Zeeman term $H_Z = \pm\mu_B B_0 \mathbb{I}$ is added to Hamiltonian (5), where $\mathbb{I}$ is the 3×3 identity matrix and the g factor is assumed to be 2. Since $[H_3, H_Z] = 0$, the uniform magnetic field does not change the dynamics of AQT of either the up or down channel. Its only effect is to generate a phase difference $\Delta \equiv 2\mu_B B_0 T/\hbar$ between them, similar to the Aharonov-Bohm interferometer [25]. Thus, if AQT is perfect, i.e., on resonance or in the adiabatic limit, qubit 3 is disentangled from qubits 1 and 2. The initial state $|\psi_1(0)\rangle = a|0\rangle + b|1\rangle$ of qubit 1 would be transferred to qubit 3 with a rotation around the z-axis by the angle Δ, $|\psi_3(T)\rangle = a|0\rangle + b\,e^{i\Delta}|1\rangle$. The fidelity $F = |\langle\psi_T|\psi_3\rangle|^2$, measured against the original target state $|\psi_T\rangle = a|0\rangle + b|1\rangle$, is given by

$$F = |a|^4 + |b|^4 + 2|a|^2|b|^2\cos\Delta$$
$$= 1 - \frac{\sin^2\theta}{2}(1 - \cos\Delta). \qquad (16)$$

where $a = \cos\frac{\theta}{2}$ and $b = \sin\frac{\theta}{2}\,e^{i\phi}$, and θ and ϕ represent the azimuthal and polar angles of the qubit state $|\psi_1(0)\rangle$ on the Bloch sphere. Note that Eq. (16) is nothing but the intensity in two-slit interference experiment [26]. If AQT is not perfect, the upper bound of the fidelity (16) is the fidelity in the absence of external magnetic fields, as shown in Fig. 5. In short, AQT in a uniform magnetic field teleports a rotated quantum state. Therefore, a modified fidelity $F' = \langle\psi'_T|\rho_3(T)|\psi'_T\rangle$ between the rotated target state $|\psi'_T\rangle = a|0\rangle + b\,e^{i\Delta}|1\rangle$ and the density matrix ρ_3 of qubit 3 takes exactly the same form as the fidelity F in the absence of the external magnetic field, as plotted in Fig. 5.

Random external magnetic fields cause spin qubits to decohere, and the AQT to lose fidelity, similar to quantum teleportation through a noisy channel [27]. While solving the AQT problem in the presence of magnetic-noise-induced decoherence in general would require an understanding of the full dynamics of the whole system-environment, for the basic physical picture it is instructive to consider first the effects on the fidelity (16) of a
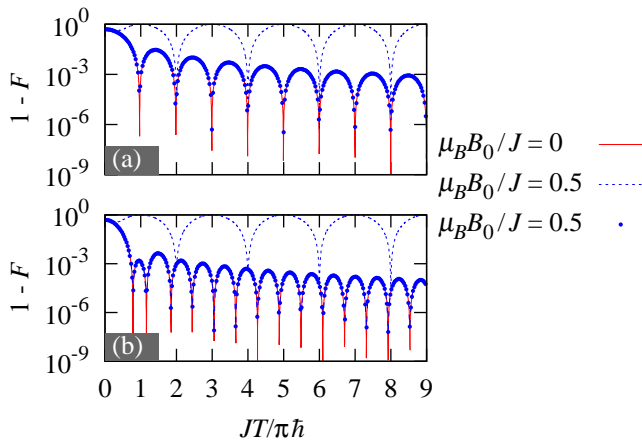
Figure 5: (color online). Infidelity $1 - F$ is plotted as a function of $JT/\pi\hbar$ for (a) XX and (b) Heisenberg couplings when a uniform magnetic field B_0 is applied. At $\mu_B B_0/J = 0.5$ the infidelity and the modified infidelity are represented by dashed blue lines and blue dots, respectively. The modified infidelity (blue dots) when $B_0 \neq 0$ is identical to the infidelity $1 - F$ (red solid lines) when $B_0 = 0$. The input state is an equal superposed state $|\psi_1\rangle = \frac{1}{\sqrt{2}}(|0\rangle + |1\rangle)$.

simple random variation $\delta B \, \hat{\mathbf{z}}$ on top of a uniform applied field. This field variation produces a random phase $\delta \equiv 2\mu_B T \delta B/\hbar$, so the total phase difference between up and down channels becomes $\Delta' = \Delta + \delta$. The effect of the random magnetic field is picked up by the modified fidelity $F' = \langle\psi'_T|\rho_3(T)|\psi'_T\rangle$. On resonance or in the adiabatic limit, it takes the form

$$F'(\theta) = 1 - \frac{\sin^2\theta}{2}(1 - \cos\delta). \qquad (17)$$

The average fidelity $\bar{F}$ over all possible input states can be obtained as

$$\bar{F}' = \frac{1}{4\pi} \int F'(\theta) \sin\theta \, d\theta \, d\phi = \frac{2}{3} + \frac{1}{3}\cos\delta. \qquad (18)$$

The phase uncertainty δ grows over evolution time T, and may range from 0 to 2π for sufficiently large T. In this case, the average of $\bar{F}'$ over $0 \leq \delta \leq 2\pi$ is given by

$$\langle\bar{F}'\rangle = \frac{2}{3} + \frac{1}{3}\langle\cos\delta\rangle = \frac{2}{3}. \qquad (19)$$

The average fidelity $2/3$ is the lower bound of the perfect AQT protocol when the noise is anisotropic [27].

Let us now consider a concrete situation where the field uncertainty is 1 Gauss. If the exchange coupling can reach 1 μeV, the resonance condition dictates that $T \sim 2n$ ns with $n \in \mathbb{N}$. The magnetic phase uncertainty at the fifth resonance peak, i.e., $T \sim 10$ ns would then be $\delta \sim 10^{-3}$. The average fidelity is thus $\bar{F}' > 1 - 10^{-6}$, which is still very high. In other words, the resonances can survive in the presence of a small magnetic uncertainty and a reasonably short evolution time. It is important to point

out, however, that off resonance, the AQT fidelity will be further reduced because then qubit 3 is not completely disentangled from qubits 1 and 2 even after the end of the protocol. Therefore, in the presence of a small uniform magnetic noise and for reasonably short T (which could still be much longer than $\hbar/J$), the infidelity curves in Fig. 3 would shift upward, and the resonance dips would not reach all the way down to zero.

In semiconductor spin qubit systems, an important decoherence channel is the magnetic noise from hyperfine interaction with the nuclear spins. Since nuclear spin dynamics is slow, while resonant AQT is quite fast, with transfer times in the order of tens of nanoseconds, the most significant effect of the hyperfine interaction in the context of AQT is in the form of an inhomogeneous random nuclear field. In other words, δB_i is different on each quantum dot and for each spin, but is static during the AQT process. For example, in the case of GaAs quantum dots, the magnetic field uncertainty is on the order of 2 mT, or about 50 neV. If the interdot exchange coupling is up to a few μeV, then $\mu_B \delta B/J \sim 10^{-2}$. In the presence of such non-uniform magnetic fields, the Zeeman Hamiltonian H_Z is still diagonal, but it no longer commutes with H_3. Thus, the dynamics of AQT would be modified. We solve this problem numerically, and show some of the results in Fig. 6. The resonance peaks become blunter and the average value of the infidelity oscillations grows over time. When $\mu_B \delta B_i/J \sim 10^{-2}$, the infidelity could be less than 10^{-3} only at the first few resonance peaks. Clearly, the resonant AQT is less robust in the presence of nonuniform random magnetic noises than uniform ones.

The above results indicate that in the presence of magnetic noise, the fidelity for AQT is much worse in the adiabatic limit than at the short-time resonances, regardless of whether the noise is uniform. Indeed, the increase in phase uncertainty over time would render the original AQT proposal of Ref. 18 completely ineffective. Instead, using resonances at short times becomes a viable solution to obtain high fidelity AQT. Practically, the best system to realize resonant AQT might be a material system such as isotropically purified Si, where the nuclear field noise is minimized, and no applied magnetic field is needed to overcome the inhomogeneous broadening due to nuclear spins.

Another major potential decoherence channel for exchange-coupled quantum dots is fluctuations in the exchange coupling itself, whether due to charge noise [31] or electron-phonon interaction [32]. Fluctuations in J would affect the AQT protocol as well. This can be most clearly seen from Fig. 4. Changes in J would lead to changes in both the direction and magnitude of the effective field experienced by the spin-1 object in Fig. 4, leading to a different precession axis and period. The system then would not return to the ground state at the expected time. Similar to the discussion above on the magnetic noise, in the presence of exchange noise, the infidelity curves in Fig. 3 would shift upward, and the resonance dips would not reach zero. It is important to
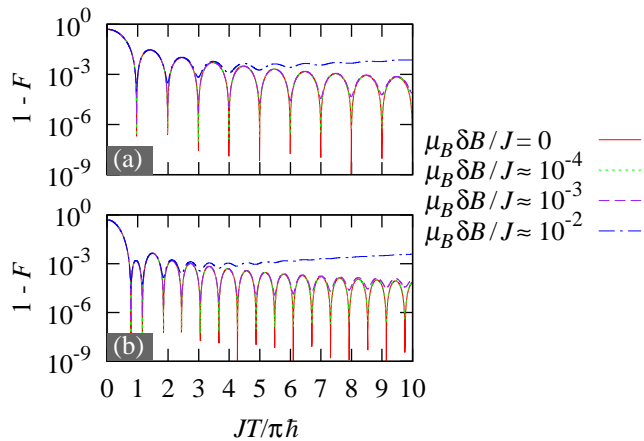
Figure 6: (color online). Modified infidelity $1-F'$ is plotted as a function of $JT/\pi\hbar$ for (a) XX and (b) Heisenberg couplings when random magnetic fields δB_i are applied. The input state is an equal superposed state $|\psi_1\rangle = \frac{1}{\sqrt{2}}(|0\rangle + |1\rangle)$.

note here that exchange noise affects all protocols that depend on the exchange interaction. In this respect AQT is not unique, and is not immune to such effects.

Our results can be tested experimentally using current technology. Controllable three-qubit systems have been demonstrated in quantum dots [10] and superconductors [19]. Single-shot measurements and the preparation of singlet states are almost routine [29]. AQT could therefore be implemented as follows. Qubit 1 is initially prepared in the "up" state, while qubits 2 and 3 are prepared in a singlet state. After switching f and g according to the AQT protocol, qubit 3 is measured. Repeating this experiment many times provides a fidelity estimate for AQT, over the evolution period T. The resonant peaks of the fidelity can be examined in the time domain by varying T. Since AQT corresponds to two parallel APs for the two spin components of a qubit, we could also explore interesting phenomena like coherent population trapping and electromagnetically induced transparency [30], which have also been studied in the context of AP, for three-level atoms.

So far we have only explored AQT with three qubits, where qubits 2 and 3 are initially in a singlet state – the same initial state used for conventional quantum teleportation. An interesting next step would be to study AQT over longer distances. Our preliminary numerical studies suggest that AQT could be implemented in a more general spin chain geometry. We leave this for future work.

In conclusion, we have shown that adiabatic quantum teleportation consists of two adiabatic passages corresponding to the quantum information transfer of "up" and "down" components of a qubit. When this protocol is performed non-adiabatically, resonances occur in the fidelity, in analogy with magnetic spin resonance. The observation of resonances points toward a new paradigm for fast and robust adiabatic gates. Our results can be tested experimentally using superconducting or spin qubits, with currently available technologies.

[1] P. W. Shor, Phys. Rev. A **52**, R2493 (1995).

[2] J. Preskill, Proc. R. Soc. A **454**, 385 (1998).

[3] B. P. Lanyon, C. Hempel, D. Nigg, M. Müller, R. Gerritsma, F. Zähringer, P. Schindler, J. T. Barreiro, M. Rambach, G. Kirchmair, M. Hennrich, P. Zoller, R. Blatt, and C. F. Roos, Science **334**, 57 (2011).

[4] A. Messiah, *Quantum Mechanics*, (North-Holland Publishing Company, Amsterdam,1963).

[5] L. D. Landau, Phys. Z. Sowjetunion **2**, 46 (1932).

[6] C.M. Zener, Proc. R. Soc. London A **137**, 696 (1932).

[7] E. C. G. Stückelberg, Helv. Phys. Acta **5**, 369 (1932).

[8] E. Majorana, Nuovo Cimento **9**, 43 (1932).

[9] W. D. Oliver, Y. Yu, J. C. Lee, K. K. Berggren, L. S. Levitov, and T. P. Orlando, Science **310**, 1653 (2005).

[10] L. Gaudreau, G. Granger, A. Kam, G. C. Aers, S. A. Studenikin, P. Zawadzki, M. Pioro-Ladrière, Z. R. Wasilewski, and A. S. Sachrajda, Nat. Phys. **8**, 54 (2012).

[11] J. Oreg, F. T. Hioe, and J. H. Eberly, Phys. Rev. A **29** 690 (1984).

[12] K. Bergmann, H. Theuer, and B. W. Shore, Rev. Mod. Phys. **70**, 1003 (1998).

[13] P. Král, I. Thanopulos, and M. Shapiro, Rev. Mod. Phys. **79**, 53 (2007).

[14] B. W. Shore, Acta Physica Slovaca **58**, 243 (2008).

[15] Y.-x. Liu, J. Q. You, L. F. Wei, C. P. Sun, and F. Nori, Phys. Rev. Lett. **95**, 087001 (2005); L.F. Wei, J. R. Johansson, L. X. Cen, S. Ashhab, and F. Nori, *ibid.* **100**, 113601 (2008).

[16] A. D. Greentree, J. H. Cole, A. R. Hamilton, and L. C. L. Hollenberg, Phys. Rev. B **70**, 235317 (2004).

[17] E. Farhi, J. Goldstone, S. Gutmann, J. Lapan, A. Lundgren, and D. Preda, Science **292**, 472 (2001).

[18] D. Bacon and S. T. Flammia, Phys. Rev. Lett. **103**, 120504 (2009).

[19] M. Mariantoni, H. Wang, R. C. Bialczak, M. Lenander, E. Lucero, M. Neeley, A. D. O'Connell, D. Sank, M. Weides, J. Wenner, T. Yamamoto, Y. Yin, J. Zhao, J. M. Martinis, and A. N. Cleland, Nat. Phys. **7**, 287 (2011).

[20] R.S. Whitney, M. Clusel, and T. Ziman, Phys. Rev. Lett. **107**, 210402 (2011).

[21] N. Datta, G. Ghosh, and M. H. Engineer, Phys. Rev. A **40**, 526 (1989).

[22] The problem can also be solved using a SU(2) group method; see C. E. Carroll and F. T. Hioe, Phys. Rev. A **42**, 1522 (1990).

[23] C. P. Slichter *Principle of Magnetic Resonance*, 3rd ed.,

(Springer-Verlag, NY, 1989).

[24] C. Cohen-Tannoudji, B. Dui, and F. Laloë, *Quantum Mechanics* (John Wiley & Sons, NY, 1977).

[25] Phys. Rev. **115**, 485 (1959).

[26] R.P. Feynman, R.B. Leighton, and M. Sands *The Feynman Lectures on Physics* Vol. III (Addison-Wesley, MA, 1965)

[27] S. Oh, S. Lee, and H.-W. Lee, Phys. Rev. A **66**, 022316 (2002).

[28] A study on AQT dynamics under decoherence with the master equation will be shown else where.

[29] I. Buluta, S. Ashhab, and F. Nori, Rep. Prog. Phys. **74**, 104401 (2011).

[30] M. O. Scully and M. S. Zubairy, *Quantum Optics*, (Cambridge Univ. Press, Cambridge, England, 1997).

[31] X. Hu and S. Das Sarma, Phys. Rev. Lett. **96**, 100501 (2006).

[32] X. Hu, Phys. Rev. B **83**, 165322 (2011).